Article

Discovery Medicine 2024; 36(181): 372–384
https://doi.org/10.24976/Discov.Med.202436181.35

Down-Regulation of *INSR* Restores Th17/Treg Immune Balance and Alleviates Airway Hyperviscosity in Asthmatic Mice via Inactivation of STAT3 Pathway

Xuanlin Jin[1], Jin Wang[2,*]

[1]Laboratory Medical College, Wenzhou Medical University, 325006 Wenzhou, Zhejiang, China
[2]Department of Pediatric, Beiyuan Community Health Service Center in Yiwu, 322000 Jinhua, Zhejiang, China
*Correspondence: wangjin7012@163.com (Jin Wang)
Published: 20 February 2024

Background: Allergic asthma (AA) is a prevalent chronic airway inflammation disease. In this study, this study aims to investigate the biological functions and potential regulatory mechanisms of the insulin receptor (*INSR*) in the progression of AA.
Methods: BALB/c mice (n = 48) were randomly divided into the following groups: control group, AA group, AA+Lentivirus (Lv)-vector short hairpin RNA (shRNA) group, AA+Lv-vector group, AA+Lv-*INSR* shRNA group, and AA+Lv-*INSR* group. The pulmonary index was calculated. mRNA and protein expression levels of *INSR*, signal transducer and activator of transcription 3 (STAT3), Janus kinase 2 (JAK2), phosphorylated-STAT3 (p-STAT3), phosphorylated-JAK2 (p-JAK2), alpha-smooth muscle actin (α-*SMA*), febrile neutropenia (*FN*), mucin 5AC (*MUC5AC*), and mucin 5B (*MUC5B*) were examined using reverse-transcription quantitative PCR (RT-qPCR) and western blot assays. Positive expressions of *INSR*, retinoic acid-related orphan receptor gamma-t (RORγt), and forkhead box protein P3 (Foxp3) were quantified by immunohistochemistry. Fluorescence intensities of α-SMA and FN were detected by immunofluorescence. Pathological morphology was observed through hematoxylin-eosin (H&E) staining, Masson staining, and Periodic Acid-Schiff (PAS) staining. Contents of immunoglobulin E (IgE), interleukin-6 (IL-6), eotaxin, interleukin-4 (IL-4), interleukin-13 (IL-13), interferon-γ (IFN-γ), interleukin-17 (IL-17), and interleukin-10 (IL-10) were quantified using enzyme-linked immunosorbent assay (ELISA). The percentage of T helper 17 (Th17) and regulatory T (Treg) cells was determined through flow cytometry.
Results: Compared to the control group, expression levels of *INSR*, p-STAT3, p-JAK2, α-*SMA*, *FN*, *MUC5AC*, *MUC5B*, RORγt, and Foxp3, as well as IgE, IL-6, eotaxin, IL-4, IL-13, and IL-17 contents, pulmonary index, glycogen-positive area (%), and Th17 cell percentage significantly increased ($p < 0.05$). Additionally, pulmonary histopathological deterioration and collagen deposition were aggravated, while Treg cell percentage and IFN-γ and IL-10 contents remarkably decreased ($p < 0.05$). The overexpression of *INSR* further exacerbated the progression of allergic asthma, but the down-regulation of *INSR* reversed the trends of the above indicators.
Conclusions: The down-regulation of *INSR* alleviates airway hyperviscosity, inflammatory infiltration, and airway remodeling, restoring Th17/Treg immune balance in AA mice by inactivating the STAT3 pathway.

Keywords: allergic asthma; *INSR*; STAT3 pathway; Th17/Treg immune balance; airway hyperviscosity

Introduction

Bronchial asthma, a chronic respiratory disease characterized by heterogeneity, includes various phenotypes, with allergic asthma (AA) being the most prevalent. The incidence of AA increased year by year [1,2]. Presently, there are approximately 334 million AA patients worldwide [3], with children constituting about half of the total incidence [4]. According to the survey, the total number of asthma patients in China is 45.7 million [5,6], of which a prevalence rate of 1.81% in adults and 4.9% in children [7]. Asthma is characterized by recurrent episodes and prolonged duration, significantly impacting both the physical and mental health of patients and imposing a substantial economic burden on their families [8]. Consequently, in-depth research into the pathogenesis of AA and the exploration of new molecular markers are essential for the improvement of AA treatment.

The insulin receptor (*INSR*) is a transmembrane protein widely distributed on the cell membrane of various tissues in the body, belonging to both the tyrosine kinase family and the insulin growth factor family [9,10]. Comprising two α-subunits and two β-subunits, *INSR* is primarily responsible for receiving extracellular insulin signals. Upon insulin stimulation, molecules associated with the insulin receptor signaling pathway undergo a series of phosphorylation and dephosphorylation reactions, sequentially transmitting and amplifying insulin signals. This process influences organs such as the liver, skeletal muscle, and adipose

tissue, ultimately exerting biological effects on the regulation of glucolipid metabolism [9,11]. Studies have revealed a close association between *INSR* and various lung diseases, including lung adenocarcinoma [12], smoking-induced lung cancer [13], and non-small cell lung cancer [14]. Additionally, a bioinformatics study identified a significant correlation between *INSR* and severe asthma [15]. However, the specific role of *INSR* in AA is not yet known and requires further elucidation in our study.

The Janus kinases 2/signal transducer and activator of transcription 3 (JAK2/STAT3) pathway plays a crucial role in regulating the occurrence and development of many diseases [16,17]. The development of asthma is also closely linked to the persistent activation of the JAK2/STAT3 pathway [18,19]. Current *in vitro* study has confirmed that inhibiting the activation of JAK2/STAT3 pathway hinders autophagy in airway smooth muscle cells [18]. Additionally, *in vivo* research has revealed that inhibiting this pathway alleviates AA by stabilizing mast cell activation [20]. These findings suggest that targeted therapy for AA targeting the JAK/STAT3 pathway holds promising application prospects. Notably, some scholars have observed *INSR* regulates arthritis symptoms in mice through the JAK2/STAT3 signaling [21].

Therefore, this study aims to elucidate the expression level of *INSR* in AA mice and focuses on the biological efficacy and potential regulatory mechanisms of down-regulating *INSR* to impede the progression of AA. These insights aim to provide new perspectives on utilizing *INSR* as a novel molecular marker for the diagnosis and treatment of allergic asthma.

Materials and Methods

Grouping and Construction of AA Model Mice

Forty-eight healthy female BALB/c mice (6–8 weeks old, 18–20 g) were obtained from Beijing Biocisco Biomedical Technology Co., Ltd. (Beijing, China) and acclimated under specific pathogen-free conditions for one week. The mice were then categorized into six groups: the control group, the AA group, the AA+Lentivirus (Lv)-vector short hairpin RNA (shRNA) group, the AA+Lv-vector group, the AA+Lv-*INSR* shRNA group, and the AA+Lv-*INSR* group. With the exception of the control group (n = 6), the remaining 42 mice were induced with ovalbumin (OVA, A21772, Sigma, St. Louis, MO, USA) to establish the allergic asthma mouse model [22,23]. On the 0th and 14th days, mice were intraperitoneally injected with 0.2 mL of freshly prepared OVA sensitization solution (containing 20 µg OVA and 1 mg aluminum hydroxide gel adjuvant in phosphate-buffered saline (PBS) solution). In contrast, the mice in the control group received equal amounts of sterilized PBS solution. Starting from the 21st day of modeling, mice were placed in a Turbo BOY N nebulizer (085G1205, PARI, Starnberg, Germany) and nebulized with 1% OVA. Simultaneously, mice in the control group were nebulized with PBS once a day for 30 minutes, for three consecutive days. Successfully induced AA mice exhibited symptoms such as shortness of breath, restlessness, and abdominal cramps. In total, 40 mice were successfully established as the model mice.

Moreover, Genepharma (Shanghai, China) was enlisted to design shRNA and construct the corresponding lentiviral vector, with the titer adjusted to 1×10^8 IU/mL. On the 17th day of modeling, 200 µL of the corresponding lentivirus suspension was administered through tail vein injection in the AA+Lv-vector shRNA group, AA+Lv-*INSR* shRNA (5′-CGTCTGGCTATACCATGAATT-3′) group, AA+Lv-vector group, and AA+Lv-*INSR* group. Conversely, mice in the control and AA groups were injected with equal amounts of PBS solution via tail vein injection.

Acquisition of Samples and Pulmonary Index

Twenty-four hours after the final nebulization, three mice were randomly selected from each group, weighed, and then intraperitoneally anesthetized with 2% sodium pentobarbital (50 mg/kg). Subsequently, the mice were euthanized by spinal dislocation. A volume of 1 mL of blood samples was collected via eyeball blood sampling. The chest cavity was promptly opened to extract the intact lungs, carefully removing the hilar lymph nodes and trachea, and aspirating any blood on the lung surface. The lung tissues were then weighed, and lung indexes were calculated using the formula: lung index = mouse lung weight (g) / mouse body weight (g) × 100%. Following weighing, the lung tissues were immediately stored at –80 °C. Additionally, the blood samples from each group were allowed to rest at 4 °C for 2 hours, followed by centrifugation at 3000 rpm for 15 minutes, and only the serum was preserved at –80 °C.

Again, 24 hours after the final nebulization, the remaining mice were euthanized. The chest cavity was opened, and the right lungs of the mice were ligated. The anterior cervical trachea was exposed, and a modified tracheal intubation needle was inserted. The left lungs were then repeatedly washed and recovered with 1 mL of PBS, and this process was repeated three times to obtain the bronchoalveolar lavage fluid (BALF). The BALF was centrifuged at 1200 rpm for 10 minutes, and both the supernatant sample and cell pellet were saved for subsequent cell counting and enzyme-linked immunosorbent assay (ELISA) analysis. Additionally, the right lung tissues were cut and immersed in a 4% paraformaldehyde solution for 3 days. Subsequently, the tissues were dehydrated through graded alcohol, cleared with xylene, and embedded in paraffin. Finally, 5 µm sections were prepared for subsequent histological staining.

Western Blot

Lung tissue weighing 50 mg was minced and lysed on ice using radio immunoprecipitation assay (RIPA) lysis

buffer (P0013B, Beyotime, Shanghai, China). The lysate was then centrifuged at 1200 rpm for 5 minutes at 4 °C, and the resulting supernatant was saved for western blot detection. Following quantification of the protein concentration with the bicinchoninic acid (BCA) kit (P0010, Beyotime, Shanghai, China), sodium dodecyl sulfate polyacrylamide gel electrophoresis (SDS-PAGE) was conducted. The target proteins, including INSR, STAT3, alpha-smooth muscle actin (α-SMA), phosphorylated-STAT3 (p-STAT3), JAK2, mucin 5AC (MUC5AC), phosphorylated-JAK2 (p-JAK2), febrile neutropenia (FN), and mucin 5B (MUC5B), were subsequently transferred to polyvinylidene fluoride (PVDF) membranes. The membranes were blocked for 1 hour with 5% skim milk, then washed three times with Tris-buffered saline containing Tween 20 (TBST) and incubated with primary antibodies [anti-INSR (1:1000, ab283689), anti-STAT3 (1:2000, ab68153), anti-p-STAT3 (1:2000, ab76315), anti-JAK2 (1:5000, ab108596), anti-p-JAK2 (1:2000, ab32101), anti-α-SMA (1:1000, ab280888), anti-FN (1:2000, ab2413), anti-MUC5AC (1:20,000, ab198294), anti-MUC5B (1:250, ab77995), anti-glyceraldehyde 3-phosphate dehydrogenase (GAPDH; 1:500, ab8245), Abcam, Cambridge, UK] overnight at 4 °C. The following day, the membrane was washed with TBST, and then incubated with the secondary antibody (1:2000, ab6728, Abcam, Cambridge, UK) for 1.5 hours at room temperature. Subsequently, the electrochemiluminescence (ECL) kit (36208ES60, Yeasen Biotechnology Co., Ltd., Shanghai, China) was used for development. GAPDH was used as the internal reference, and the relative expression levels of INSR, STAT3, p-STAT3, JAK2, p-JAK2, α-SMA, FN, MUC5AC, and MUC5B were analyzed using Image Pro Plus software (Version 6.0, NIH, Bethesda, MD, USA).

Reverse-Transcription Quantitative PCR (RT-qPCR)

Lung tissue weighing 50 mg was cut into pieces and homogenized, and TRIzol reagent (15596026, Invitrogen, Carlsbad, CA, USA) was added to extract total RNA. Subsequently, complementary DNA (cDNA) was generated by reverse transcription following the protocols of the reverse transcription kit (RR047Q, TaKaRa, Dalian, China). Using the cDNA product as a template, RT-qPCR amplification was performed with the One Step RT-qPCR kit (A15300, Applied Biosystems, Foster City, CA, USA). The relative expressions of each gene were calculated using the $2^{-\Delta\Delta Ct}$ method, with beta-actin (β-actin) serving as the internal reference. The primer sequences are listed in Table 1.

Table 1. The primer sequences used in this study.

Name	Primer
INSR	F: GAAGAAATCTCAGGGTTCCTAAAG R: TTCTGGTTGTCCAAGGCGTA
α-SMA	F: CATCACCAACTGGGACGACATGGAA R: GCATAGCCCTCATAGATGGGGACATTG
FN	F: GTGTTGGGAATGGTCGTGGGGAATG R: CCAATGCCACGGCCATAGCAGTAGC
MUC5AC	F: TCAACGGAGACTGCGAGTACAC R: TCTTGATGGCCTTGGAGCA
MUC5B	F: CTGCGAGACCGAGGTCAACATC R: TGGGCAGCAGGAGCACGGAG
β-actin	F: CGCACGAGATTGAGCAATAA R: GTACAAAGGGCAGGGACGTA

Note: *INSR*, insulin receptor; *α-SMA*, alpha-smooth muscle actin; *FN*, febrile neutropenia; *MUC5AC*, mucin 5AC; *MUC5B*, mucin 5B; *β-actin*, beta-actin.

Immunohistochemistry (IHC)

IHC was conducted to detect the positive expressions of INSR, retinoic acid-related orphan receptor gamma-t (RORγt), and forkhead box P3 (Foxp3) proteins in lung tissue. The lung tissue sections were deparaffinized, followed by immersion in 0.01 M citrate buffer, and antigen retrieval was performed using a microwave. Next, primary antibodies [anti-INSR (1:2000, ab283689), anti-RORγt (1:1000, ab207082), anti-Foxp3 (1:500, ab215206), Abcam, Cambridge, UK] were added and incubated overnight at 4 °C. Sections were washed three times with PBS, followed by incubation with Goat anti-mouse IgG H&L (HRP) (1:500, ab6789, Abcam, Cambridge, UK) for 20 minutes at room temperature. After thorough PBS washing, streptavidin-biotin enzyme complex (SABC) solution (ZN1854, BioLab, Beijing, China) was added for 0.5 hours. Subsequent to another PBS rinse, 3,3′-diaminobenzidine (DAB) color-developing solution was added dropwise, and the color development was terminated by rinsing with tap water when a brownish-yellow color appeared. The tissues were counterstained with hematoxylin, differentiated using 1% hydrochloric acid alcohol, and subsequently washed with tap water. Following standard procedures, the sections were dehydrated, clarified, and sealed. For each section, six fields of view were randomly chosen, observed, and photographed using a CKX53 optical microscope (Olympus, Tokyo, Japan). Finally, quantitative analysis was conducted using Image Pro Plus software (Version 6.0, NIH, Bethesda, MD, USA).

Hematoxylin-Eosin (H&E) Staining

Five-micrometer paraffin sections of lung tissues were deparaffinized to water and washed with ddH_2O for 5 minutes. Following the instructions of the HE staining kit (E607318, Sangon Biotech, Shanghai, China), hematoxylin staining solution was applied for 8 minutes, hydrochloric acid differentiation was performed for 2 seconds, eosin staining for 5 minutes, and any excess staining solution was washed off with ddH_2O. Subsequently, the sections were dehydrated, clarified, sealed, and the pathological changes in lung tissue were observed and photographed using a CKX53 optical microscope (Olympus, Tokyo, Japan). The

extent of pathological deterioration was assessed by evaluating the numbers of peribronchiolar and perivascular infiltrating inflammatory cells. The criteria were as follows: 0 indicated the absence of cells, 1 denoted a few cells, 2 represented peribronchial cells (one cell layer) and a ring of inflammatory cells; 3 indicated peribronchial cells (two to four cell layers) and a ring of inflammatory cells; and 4 indicated peribronchial cells (more than four cell layers) and a ring of inflammatory cells.

Cell Counting

BALF cell pellets were resuspended in normal saline, and 200 µL was pipetted for Diff-Quick staining (40748ES60, Yeasen Biotechnology Co., Ltd., Shanghai, China). Subsequently, the numbers of total cells, eosinophils, neutrophils, lymphocytes, and macrophages were counted using a blood cell counter (Scepter 2.0, Millipore, Bedford, MA, USA).

Enzyme-Linked Immunosorbent Assay (ELISA)

After thawing serum and BALF supernatant samples, ELISA kits (Solarbio, Beijing, China; SEKM-0095, SEKM-0018, SEKM-0010, SEKM-0007, SEKM-0073, SEKM-0005, SEKM-0014, SEKM-0031) were utilized to measure the contents of inflammatory factors, including immunoglobulin E (IgE), interleukin-17 (IL-17), interleukin-10 (IL-10), interleukin-6 (IL-6), eotaxin, interleukin-4 (IL-4), interleukin-13 (IL-13), and interferon-γ (IFN-γ). Following the provided protocols, absorbance values at 450 nm were measured using a microplate reader. The concentrations of each inflammatory factor were then calculated based on the standard curve.

Masson Staining

Five-micrometer lung tissue sections were dewaxed to water, rinsed with ddH_2O for 3 minutes, and stained with Masson composite staining solution (G1340, Solarbio, Beijing, China) for 8 minutes. After washing with ddH_2O, phosphomolybdic acid was added for 5 minutes, and aniline blue was introduced for a 5-minute reaction. Subsequently, the differentiation solution was added to react for 30 seconds. Dehydration was carried out through gradient alcohol, followed by clarification with xylene, sealing with neutral resin, and observation and scanning using a CKX53 optical microscope (Olympus, Tokyo, Japan). The estimated percentage of the blue area to the total area on Masson-stained sections was used to assess the degree of collagen deposition in the lung tissue using Image Pro Plus software (Version 6.0, NIH, Bethesda, MD, USA).

Periodic Acid-Schiff (PAS) Staining

Five-micrometer lung tissue paraffin sections were routinely deparaffinized, oxidized with 0.5% periodic acid (C0124S, Beyotime, Shanghai, China) for 10 minutes, and then washed with PBS for 10 minutes. Subsequently, the sections were immersed in Schiff reagent for 20 minutes in dark conditions. After staining with eosin for 3 minutes, the sections were rinsed with PBS. Following this, the sections were dehydrated, clarified, mounted, observed under a CKX53 optical microscope (Olympus, Tokyo, Japan), and photographed. Glycogen deposition appeared purplish red, and the glycogen-positive area (%) was determined using Image Pro Plus software (Version 6.0, NIH, Bethesda, MD, USA).

Immunofluorescence (IF)

Paraffin sections of lung tissue were deparaffinized to water and rinsed with PBS for 15 minutes. The tissue sections were then placed into sodium citrate repair solution and heated for antigen retrieval. After cooling the sections naturally at room temperature, they were blocked for 1 hour with the gradual addition of blocking solution. Subsequently, primary antibodies anti-α-SMA (1:50, ab280888, Abcam, Cambridge, UK) and anti-FN (1:100, ab2413, Abcam, Cambridge, UK) were added and incubated at 4 °C overnight. Specific fluorescent secondary antibodies Rhodamine (TRITC) (SA00007-2, Proteintech, Wuhan, China) and CoraLite® 488 (KFA001, Proteintech, Wuhan, China) were then added and incubated for 2 hours at room temperature in the dark. The sections were placed on a decolorization shaker and washed three times with PBS. An anti-quenching sealer (S36964, Thermo Fisher Scientific, Waltham, MA, USA) containing 4′,6-diamidino-2-phenylindole (DAPI) was applied to seal the slides, and a fluorescence microscope (BX53, Olympus, Tokyo, Japan) was utilized to capture photographs of lung tissue sections.

Flow Cytometry

The lung tissue was minced, ground, and homogenized. It was then placed into a digestion solution containing 1 mg/mL collagenase III for approximately 1 hour at room temperature in the dark, and the digestion was terminated in an ice bath. Subsequently, the filtrate was collected, centrifuged at 1300 rpm for 10 minutes at 4 °C, the supernatant was discarded, and 5 mL of erythrocyte lysate was added, followed by incubation on ice for 10 minutes. The supernatant was discarded through centrifugation, and 5 mL of Roswell Park Memorial Institute (RPMI)-1640 complete medium containing double antibiotics (R8758, Sigma-Aldrich, St. Louis, MO, USA) was added to resuspend the cell pellet, creating a single-cell suspension. The cell concentration was adjusted to 2×10^6 cells/mL. All cells were verified through mycoplasma testing and STR testing. For the flow cytometry analysis, 1×10^6 lung cells were taken into a flow sample tube, and 1 mL of fluorescence-activated cell sorting (FACS) buffer was added to wash the cells, repeating the process twice.

Subsequently, a 50 µL mixture of CD4 and CD25 antibodies (560767, dilution ratio 1:200, BD Bioscience, San Jose, CA, USA) was added and incubated for 20 minutes

at 4 °C. Following this, 1 mL of FACS Buffer was added to vortex the cells. Then, 5 µL of Foxp3 (1:100) and 1.25 µL of interleukin-17A (IL-17A) (1:200) specific fluorescent antibodies were added, and the cells were incubated overnight at 4 °C.

After adding 2 mL of Wash Buffer to wash the cells, the supernatant was discarded through centrifugation. The cell pellet was then resuspended in 350 µL of flow buffer and analyzed for the percentage of T helper cell (Th17) and regulatory T (Treg) cells. Specifically, Th17 cells in lung tissue were double positive for CD4 antibody and IL-17A antibody, while Treg cells were triple positive for CD4, CD25, and Foxp3 antibody.

Statistical Analysis

The results were presented as the mean ± standard deviation (SD), and data analysis was conducted using GraphPad Prism 8.0 (GraphPad Software, San Diego, CA, USA). Comparisons were made using LSD-*t* test or one-way analysis of variance (ANOVA). A significance level of $p < 0.05$ was considered statistically significant.

Results

INSR Highly Expressed in the Lung Tissue of OVA-Induced Allergic Asthmatic Mice

As depicted in Fig. 1A,B, the expression levels of *INSR* mRNA and protein were significantly elevated in the AA group ($p < 0.05$). Additionally, pulmonary bronchial tissues from each group of mice were collected, processed into paraffin sections, and subjected to IHC. The results revealed a notable increase in the positive expression of *INSR* in the AA group (Fig. 1C, $p < 0.05$).

Down-Regulation of INSR Attenuated Pulmonary Inflammatory Cell Infiltration and Delayed Allergic Asthma Progression

We further modulated the expression levels of *INSR* to elucidate its biological role in AA progression. In comparison to the AA group, both *INSR* mRNA and protein expression levels were significantly downregulated in the AA+Lv-*INSR* shRNA group (Fig. 2A,B, $p < 0.05$), while the *INSR* mRNA and protein expression levels were notably enhanced in the AA+Lv-*INSR* group ($p < 0.05$). These results indicate the successful knockdown or overexpression of *INSR*.

Microscopically, the structure of the alveolar wall in mice from the control group was intact, with uniform alveolar size, neatly arranged alveolar epithelial cells, and no lymphocyte infiltration around the bronchi. Additionally, the mucosa was not hyperplastic or deformed.

In the AA group, the alveolar structure was severely damaged, the tracheal wall was thickened, and inflammatory cell infiltration, mainly eosinophils and lymphocytes, was evident under and around the mucosa. Additionally, the smooth muscle of the airway was significantly thickened, and a large number of epithelial cells were proliferated, deformed, and detached at the mucosa. Following the knockdown of *INSR*, inflammatory infiltration, airway smooth muscle proliferation, and epithelial cell deformation and exfoliation were all reduced (Fig. 2C). Moreover, the down-regulation of *INSR* effectively alleviated inflammation in AA mice, as indicated by a significant reduction in the number of eosinophils, total cells, neutrophils, lymphocytes, and macrophages, along with a decrease in the contents of IL-6 and eotaxin in the AA+Lv-*INSR* shRNA group (Fig. 3A, $p < 0.05$).

Furthermore, the knockdown of *INSR* significantly impeded AA progression, leading to a decrease in IgE content and pulmonary index (Fig. 3B,C, $p < 0.05$), and an improvement in pulmonary histopathology. Conversely, overexpression of *INSR* exacerbated pulmonary inflammation and accelerated the AA process. In comparison to the AA group, the AA+Lv-*INSR* group exhibited a notable increase in the number of eosinophils, total cells, neutrophils, lymphocytes, and macrophages, along with elevated levels of IgE, IL-6, eotaxin, and pulmonary index ($p < 0.05$). Additionally, the histopathology of lung tissue deteriorated in the AA+Lv-*INSR* group. Incidentally, no significant differences were observed in the indexes between the AA group, the AA+Lv-vector shRNA group, and the AA+Lv-vector group ($p > 0.05$).

Down-Regulation of INSR Improved Airway Remodeling via Inactivation of STAT3 Pathway

Increased *INSR* expression was observed in the AA model mice, and additionally, the levels of p-STAT3/STAT3 and p-JAK2/JAK2 were significantly elevated, indicating activation of the JAK2/STAT3 pathway (Fig. 4A, $p < 0.05$). Knockdown of *INSR* led to a decrease in the expression levels of p-STAT3 and p-JAK2, while upregulation of *INSR* elevated the expressions of these two proteins ($p < 0.05$).

Upon *INSR* knockdown, the degree of collagen deposition in lung tissue, as well as the expression levels of α-*SMA* mRNA and *FN* mRNA, the expressions of α-SMA and FN, and the fluorescence intensities of α-SMA and FN, significantly decreased in the AA+Lv-*INSR* shRNA group (Fig. 4B–D and Fig. 5, $p < 0.05$). This suggests that knockdown of *INSR* undoubtedly improved airway remodeling through the inactivation of STAT3 signaling. However, overexpression of *INSR* aggravated lung tissue fibrosis and worsened airway remodeling, with all indicators demonstrating an increasing trend compared to the AA group ($p < 0.05$). Notably, there was no significant difference among the AA+Lv-vector group, the AA+Lv-vector shRNA group, and the AA group ($p > 0.05$).

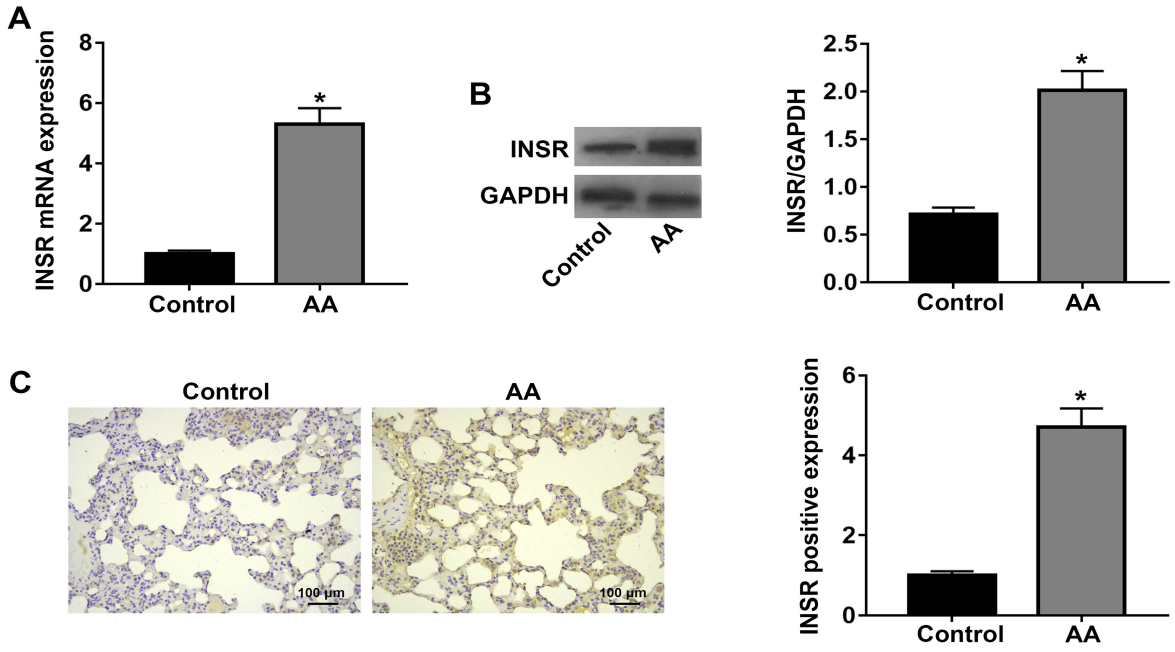

Fig. 1. High expression level of *INSR* in the lung tissue of AA mice. (A) The relative levels of *INSR* mRNA in the lung tissues (N = 3); (B) The relative expressions of INSR in the lung tissues (N = 3); (C) The positive expressions of INSR in bronchial epithelium of the lung tissues (IHC, ×400); $^{*}p < 0.05$ vs control group. AA, allergic asthma; IHC, immunohistochemistry; GAPDH, glyceraldehyde 3-phosphate dehydrogenase.

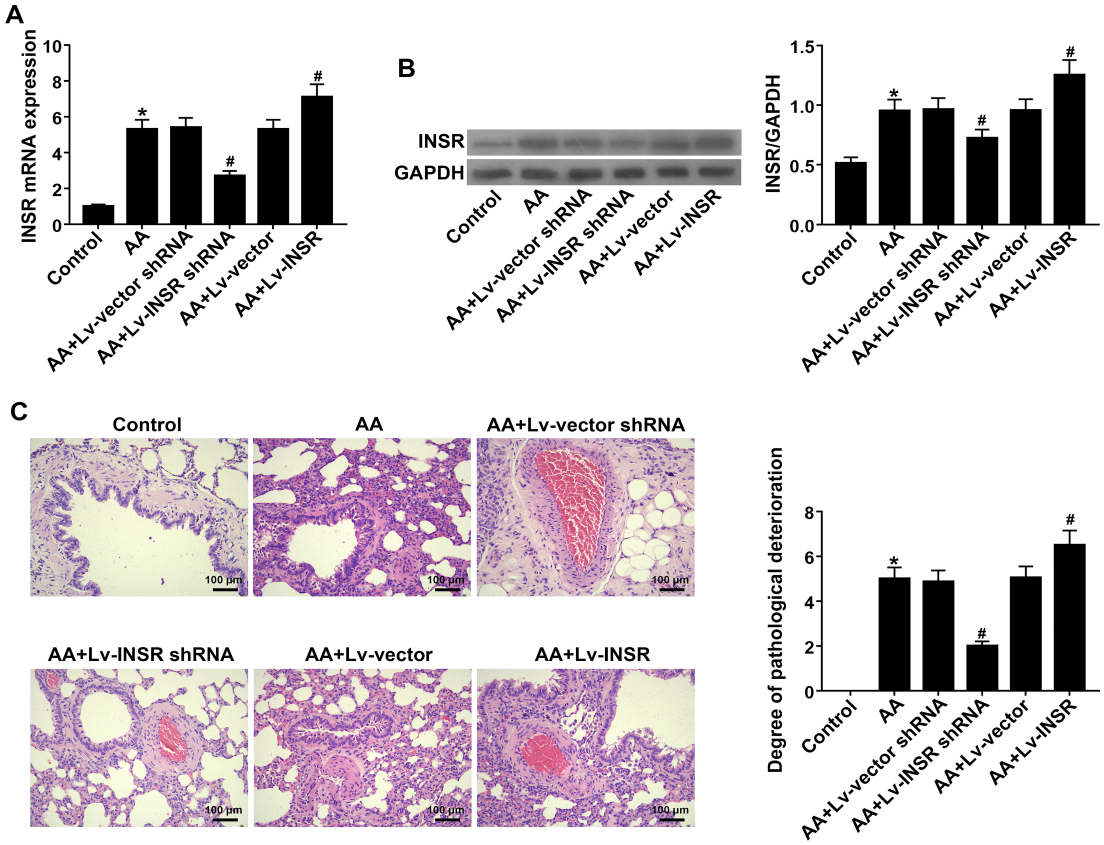

Fig. 2. Knockdown of *INSR* attenuated inflammation of AA mice. (A) The relative levels of *INSR* mRNA in lung tissue (N = 3); (B) The relative expressions of INSR in lung tissues (N = 3); (C) The pulmonary histopathology (hematoxylin-eosin (H&E) staining, ×400). $^{*}p < 0.05$ vs control group, $^{\#}p < 0.05$ vs AA group. Lv, Lentivirus; shRNA, short hairpin RNA.

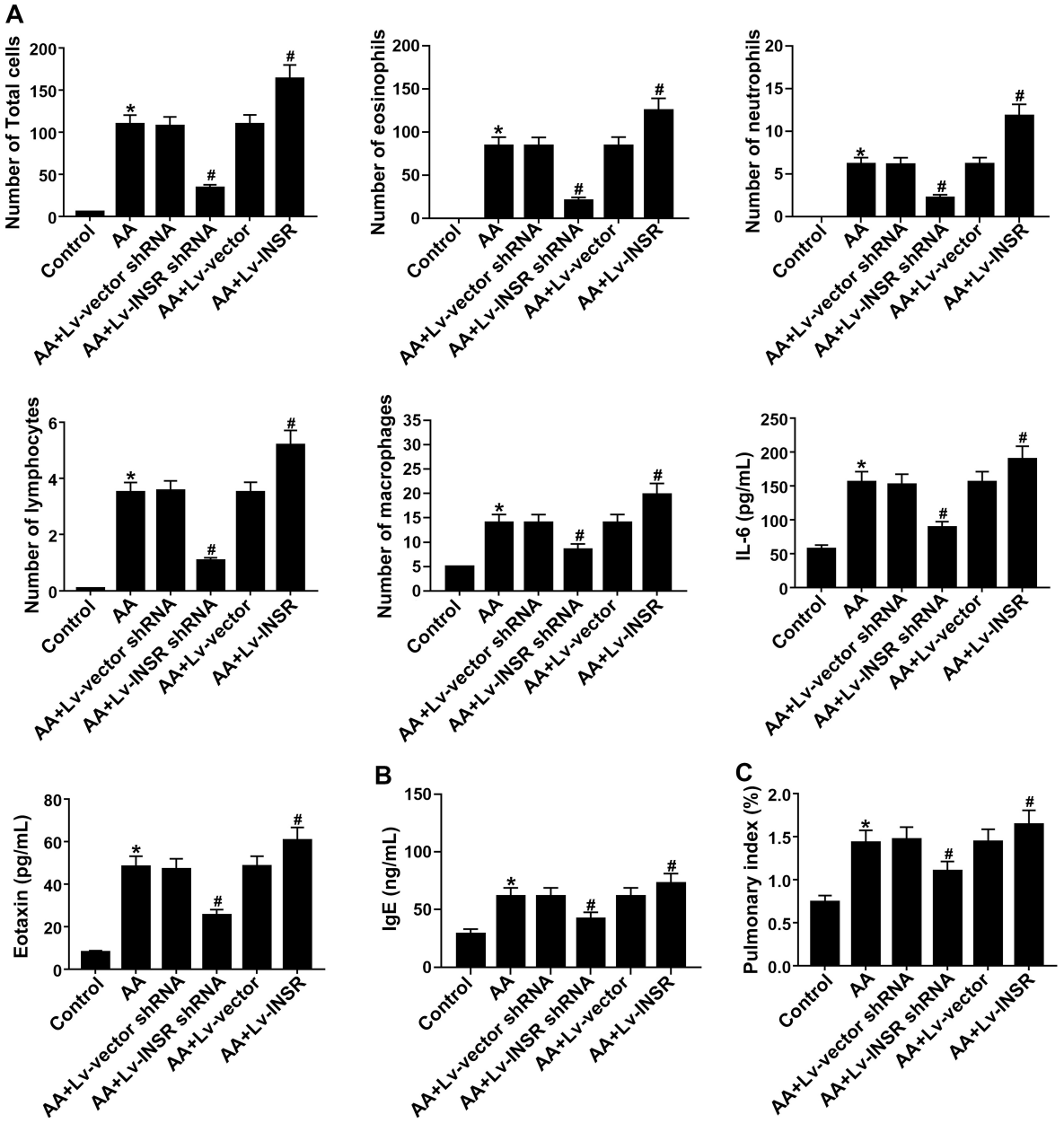

Fig. 3. Knockdown of *INSR* attenuated inflammation, IgE and pulmonary index of AA mice. (A) The number of different inflammatory cells in BALF (N = 5); (B) The content of IgE in serum in BALF (N = 5); (C) The percentage of pulmonary index (N = 3); $^{*}p < 0.05$ vs control group; $^{\#}p < 0.05$ vs AA group. IL-6, interleukin-6; IgE, immunoglobulin E; BALF, bronchoalveolar lavage fluid.

Down-Regulation of INSR Alleviated Airway Hyperviscosity

As depicted in Fig. 6A, very few goblet cells were observed in the airways and bronchi of mice in the control group, with no noticeable mucus secretion. In contrast, the AA group exhibited a significant increase in mucus and proliferation of goblet cells in the airways. Furthermore, the proliferation of bronchial goblet cells and mucus secretion in the AA+Lv-*INSR* shRNA group were markedly reduced. Additionally, the expression levels of *MUC5AC* mRNA, *MUC5B* mRNA, MUC5AC, and MUC5B, as well as the contents of IL-4 and IL-13, significantly decreased in the AA+Lv-*INSR* shRNA group compared to the AA group, but increased in the AA+Lv-*INSR* group (Fig. 6B–D, $p < 0.05$). Moreover, the IFN-γ content increased in the AA+Lv-*INSR* shRNA group, while decreased in the AA+Lv-*INSR* group ($p < 0.05$).

Down-Regulation of INSR Restored Th17/Treg Immune Balance

In comparison to normal mice, the Th17/Treg immune balance was disrupted in the AA model mice. The content of IL-17, the percentage of Th17 cells, and the positive expression of RORγt were notably elevated in the AA group,

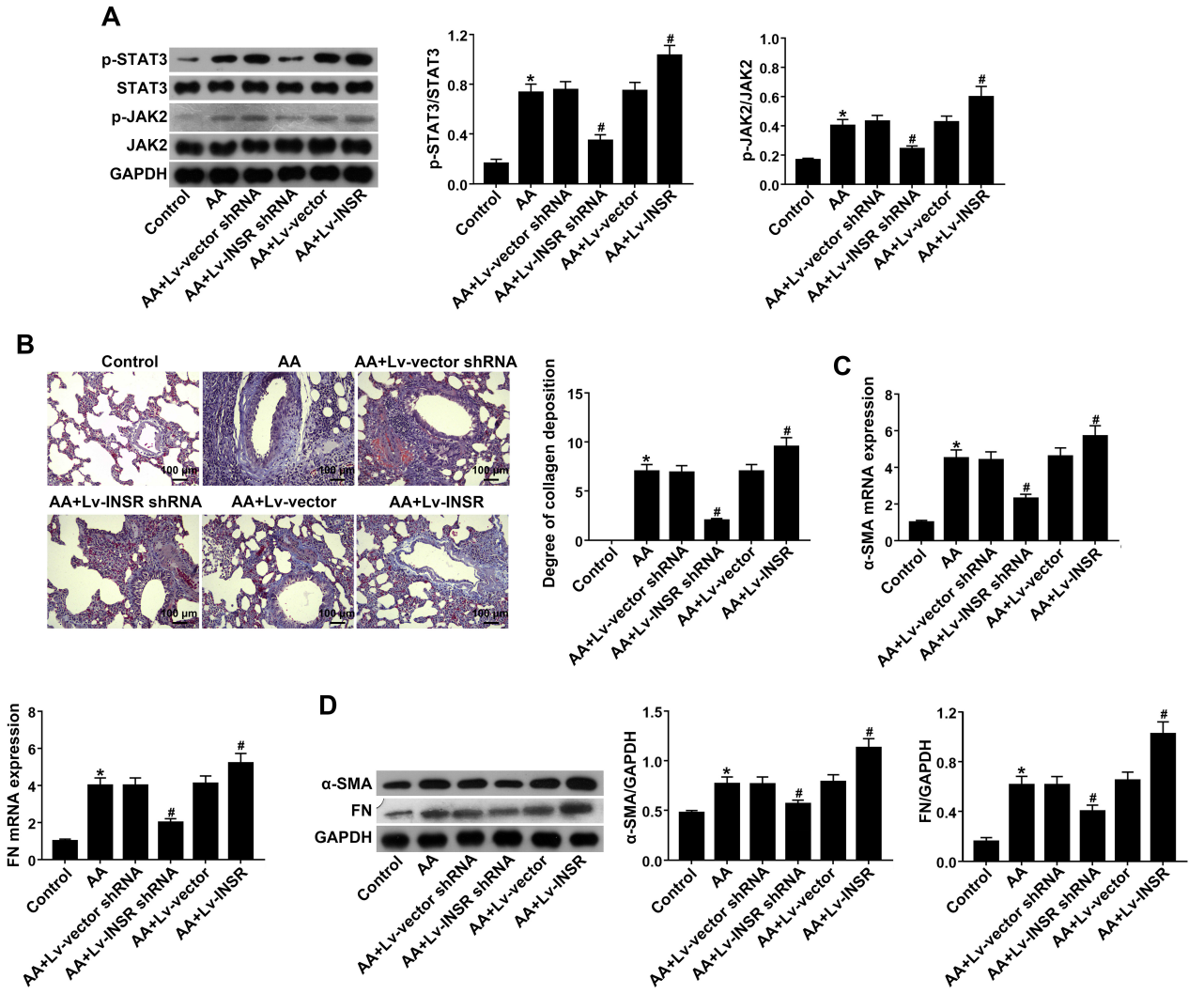

Fig. 4. Knockdown of *INSR* improved airway remodeling via inactivation of the JAK2/STAT3 signaling. (A) The relative expressions of p-STAT3, STAT3, p-JAK2, and JAK2 (N = 3); (B) The pathology of lung tissues (Masson staining, ×40); (C) The relative levels of α-*SMA* mRNA and *FN* mRNA (N = 3); (D) The relative expression of α-SMA and FN (N = 3); $^{*}p < 0.05$ vs control group; $^{\#}p < 0.05$ vs AA group. JAK2, Janus kinase 2; STAT3, signal transducer and activator of transcription 3; p-STAT3, phosphorylated-STAT3; p-JAK2, phosphorylated-JAK2.

while the content of IL-10, the percentage of Treg cells, and the positive expression of Foxp3 were declined (Figs. 7,8, $p < 0.05$). Further down-regulation of *INSR* significantly reversed the trends of the above indicators ($p < 0.05$), revealing that the Th17/Treg immune balance was restored. Nevertheless, the content of IL-17, the percentage of Th17 cells, and the positive expression of RORγt increased in the AA+Lv-*INSR* group, while the content of IL-10, the percentage of Treg cells, and the positive expression of Foxp3 decreased compared with the AA group ($p < 0.05$).

Discussion

The pathogenesis of AA has not been fully elucidated, but it has been reported to be associated with immune-inflammatory mechanisms [24]. AA is characterized by chronic bronchial inflammation and increased airway responsiveness to various stimuli. Inadequate symptom control can result in a series of changes in airway structure [25,26]. Clinical studies have identified pathophysiological changes marked by increased levels of IgE and eosinophils in the airways of AA patients, contributing to airway inflammation-a necessary condition for airway remodeling [27,28]. This is because airway inflammation leads to permanent destruction of airway tissue on one hand, and chronic lung tissue repair on the other, subsequently inducing airway remodeling [29]. The results of the current study support this perspective, as a significant increase in the number of all types of inflammatory cells in the BALF of AA mice compared to the control mice was observed. Additionally, there was a substantial increase in IgE and eotaxin (an inflammatory factor associated with eosinophil in-

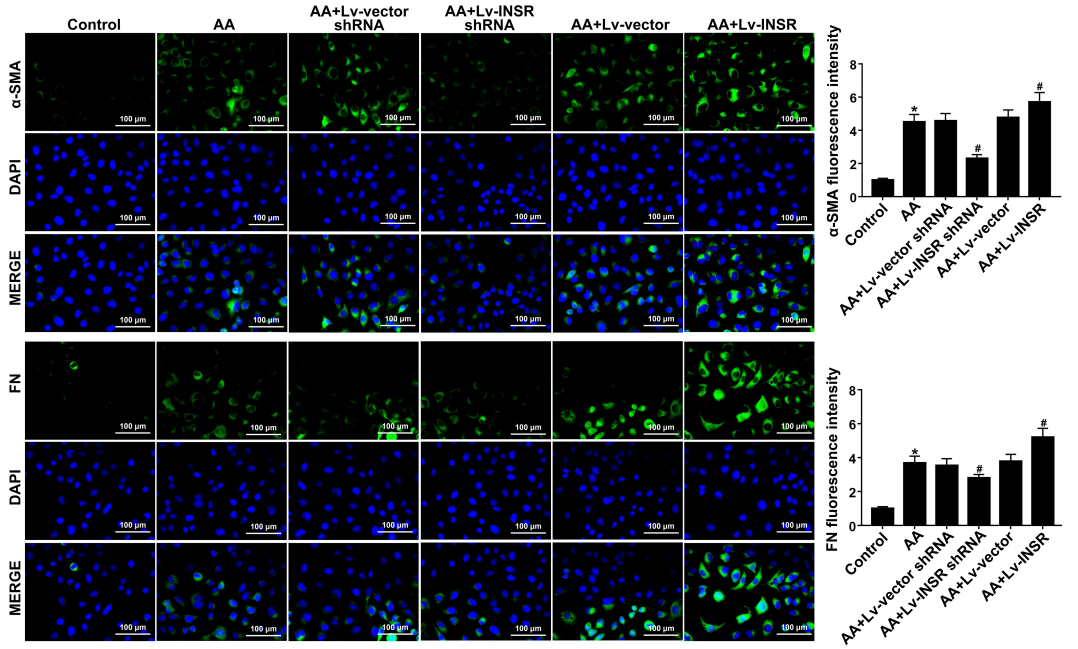

Fig. 5. Knockdown of *INSR* improved airway remodeling via inactivation of the JAK2/STAT3 signaling. The immunofluorescence (IF) intensities of α-SMA and FN (IF, $\times$400); $^{*}p < 0.05$ vs control group; $^{\#}p < 0.05$ vs AA group.

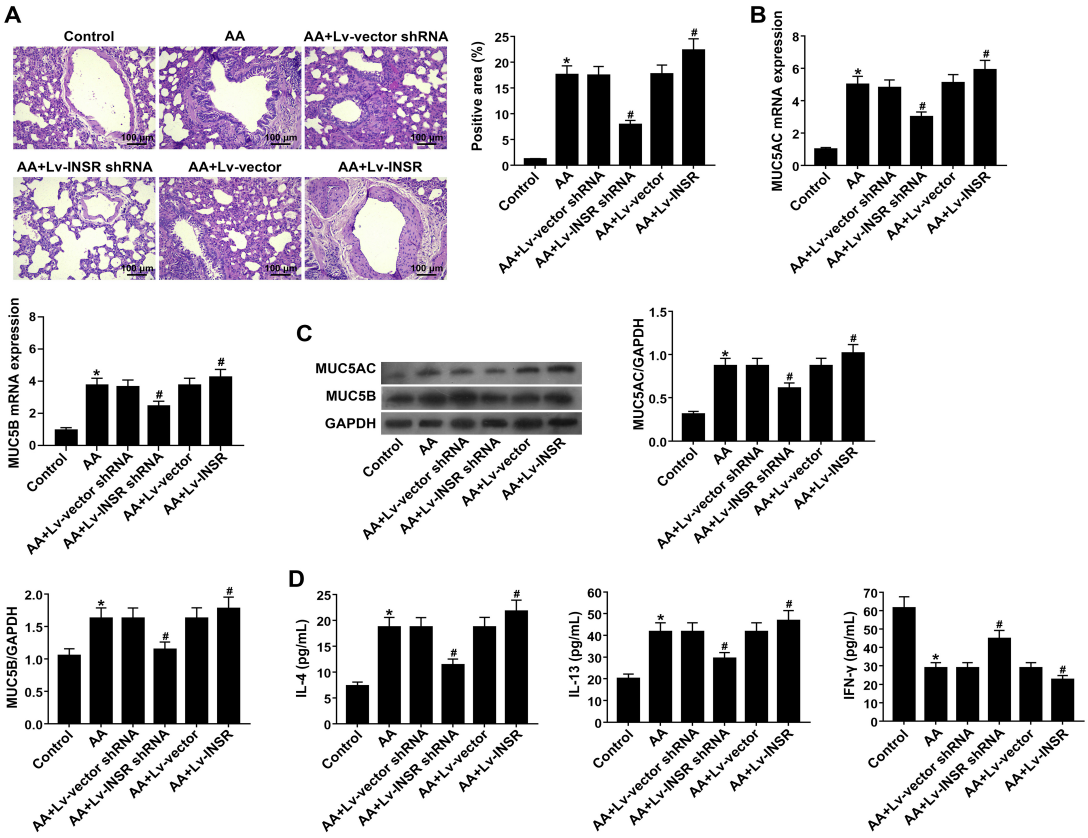

Fig. 6. Knockdown of *INSR* reduced airway hyperviscosity. (A) The bronchial goblet cell hyperplasia and mucus secretion (Periodic Acid-Schiff (PAS) staining, $\times$400); (B) The relative levels of *MUC5AC* mRNA and *MUC5B* mRNA (N = 3); (C) The relative expression of MUC5AC and MUC5B (N = 3); (D) The contents of IL-4, IL-13, and IFN-γ in BALF (N = 5); $^{*}p < 0.05$ vs control group; $^{\#}p < 0.05$ vs AA group. IL-4, interleukin-4; IL-13, interleukin-13; IFN-γ, interferon-γ.

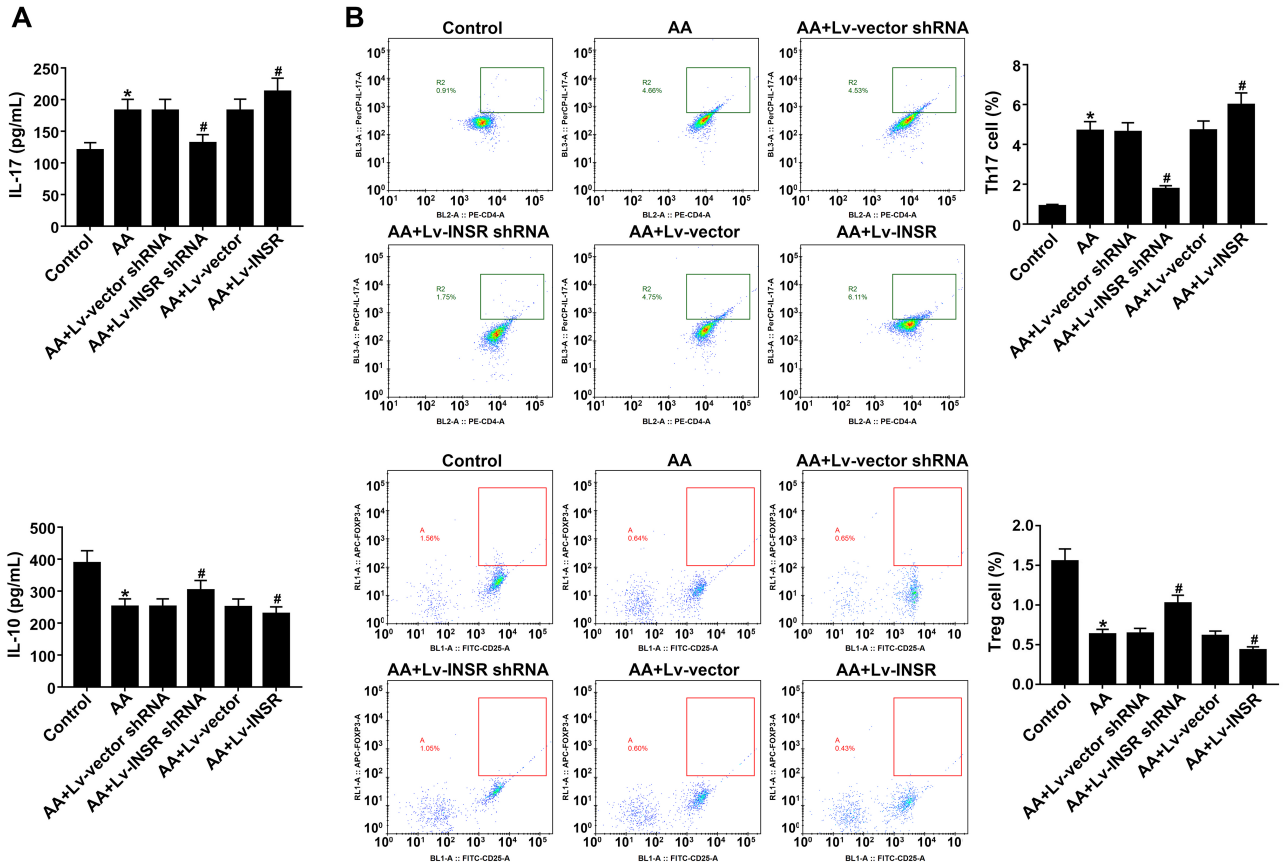

Fig. 7. Knockdown of *INSR* improved Th17/Treg immune balance. (A) The serum contents of IL-17 and IL-10 (N = 3); (B) The percentages of Th17 cells and Treg cells (N = 3); $^{*}p < 0.05$ vs control group; $^{\#}p < 0.05$ vs AA group. IL-17, interleukin-17; IL-10, interleukin-10; Th17, T helper 17; Treg, regulatory T.

filtration). Moreover, the pathological morphology of lung tissue in AA mice exhibited key features of airway remodeling, including thickening of tracheal smooth muscle, extensive submucosal infiltration of eosinophils, proliferation, deformation, and even shedding of epithelial cells, noticeable collagen deposition, and elevated expression levels of fibrosis marker proteins α-SMA and FN. Nevertheless, the deterioration of lung histopathology and airway remodeling in AA mice were alleviated through the down-regulation of *INSR*, resulting in reduced smooth muscle hyperplasia, diminished inflammatory infiltration, and reduced collagen deposition.

As a member of the receptor tyrosine kinase family, the primary physiological function of *INSR* is closely associated with insulin signaling, allowing it to play a role in the regulation of glucose metabolism through insulin signaling [30]. Additionally, the deficiency of *INSR* signaling has been shown to compromise CD4+ T cell-mediated pro-inflammatory functions by influencing T cell metabolism, including glycolysis and aerobic metabolism. This modulation ultimately enhances the host's defense against infection [31].

In this study, the knockdown of *INSR* significantly reduced the infiltration of inflammatory cells in the lung tissue of AA mice by deactivating STAT3 signaling. Additionally, there was a noticeable decrease in the levels of IgE, IL-6, IL-4, IL-13, and IL-17, while the levels of IFN-γ and IL-10 increased. Previous research has indicated that airway inflammatory cell infiltration is a characteristic feature of asthma, and the secretion of IL-4, IL-13, and IFN-γ by inflammatory cells contributes to airway inflammation and increased airway mucus secretion [32]. As a crucial component of airway mucus, mucin (MUC) plays a pivotal role in the proliferation of pathogenic bacteria, recurrent airway infections, and persistent diseases. It is also a significant factor contributing to the progressive aggravation of bronchial asthma. Specifically, *MUC5AC* and *MUC5B*, as mucins that enhance mucus secretion in the airway, are situated in the goblet cells of the airway epithelium, and their expressions are closely associated with the proliferation of airway goblet cells and mucus secretion [33]. As previously mentioned, the AA+Lv-*INSR* shRNA group mice exhibited decreased levels of IL-4 and IL-13, increased levels of IFN-γ, suppressed airway inflammation, and relieved airway hyperviscosity. Additionally, there was a significant reduction in bronchial goblet cell hyperplasia and mucus secretion in mice. The down-regulation of *INSR* corresponded with decreased expression levels of *MUC5AC* and *MUC5B*.

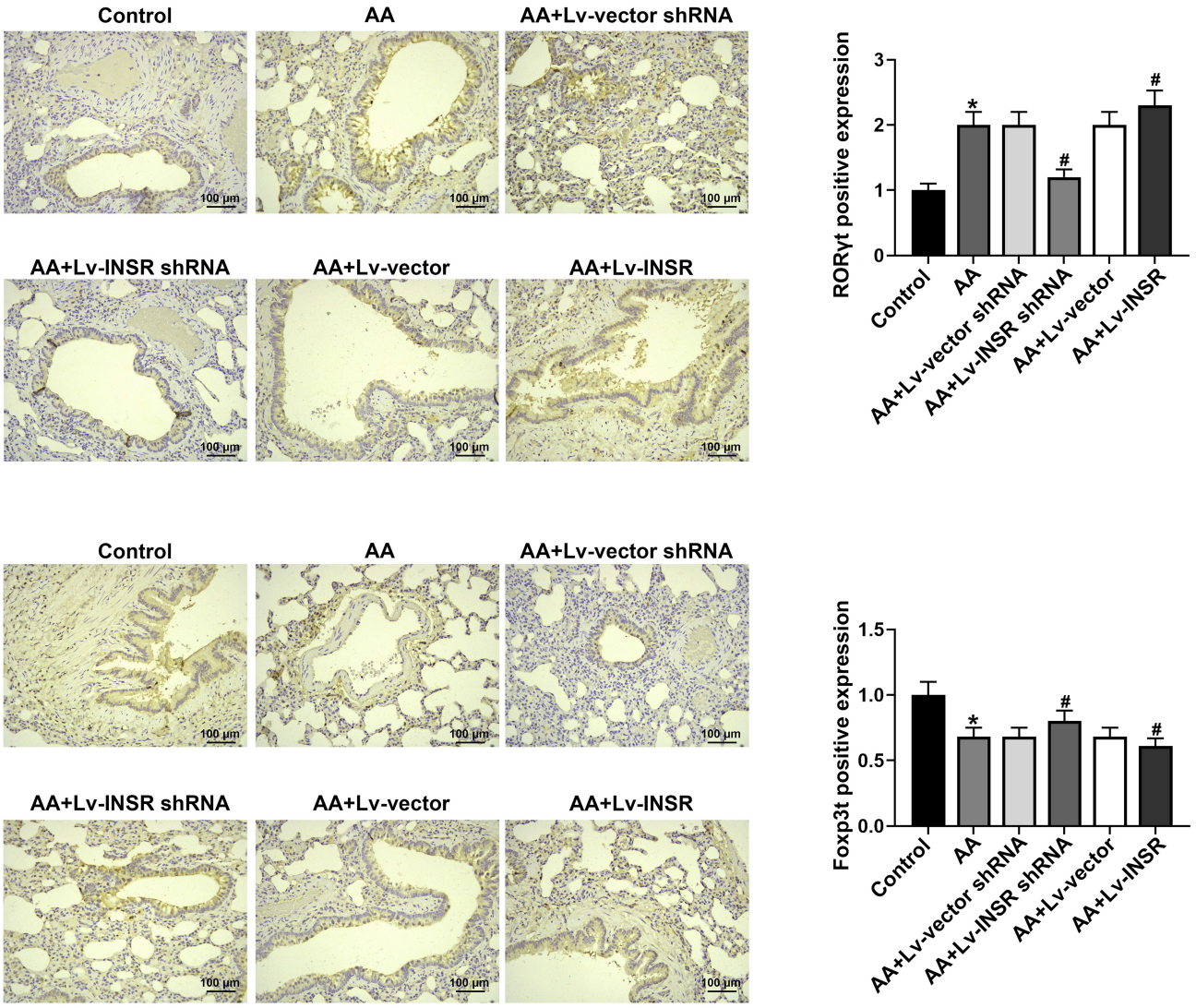

Fig. 8. Knockdown of *INSR* improved Th17/Treg immune balance. The positive expressions of RORγt and Foxp3 in lung tissues; $^{*}p < 0.05$ vs control group; $^{\#}p < 0.05$ vs AA group. RORγt, retinoic acid-related orphan receptor gamma-t; Foxp3, forkhead box protein P3.

Modern medical research has affirmed that the dynamic balance between Th17 and Treg is crucial for maintaining the relative stability of the body's immune state, and any imbalance can lead to the development of asthma [34,35]. In the presence of inflammation, CD4+T lymphocytes differentiate into Th17 cells under the combined influence of IL-6 and transforming growth factor β (TGF-β). Th17 cells, in turn, secrete IL-17, which recruits neutrophil aggregates, leading to extensive neutrophil infiltration in the airway. This process accelerates airway remodeling and mucus secretion [36,37].

Conversely, CD4+T lymphocytes differentiate into Tregs when stimulated by TGF-β alone. Treg cells, in particular, secrete the anti-inflammatory factor IL-10, directly restraining the activation of airway monocytes and eosinophils, thereby preserving host autoimmune tolerance [38]. Additionally, the specific transcription factor Foxp3 inhibits the differentiation of Th17 cells by directly interacting with RORγt. It can be asserted that restoring the Th17/Treg immune balance is pivotal in the treatment of asthma [39]. The results of our current study demonstrated that the down-regulation of *INSR* corrected the Th17/Treg imbalance in the AA+Lv-*INSR* shRNA group. Specifically, the proportion of Th17 cells and the expression levels of RORγt decreased, while the proportion of Treg cells and the expression of Foxp3 increased compared to AA mice.

Conclusions

In summary, elevated levels of *INSR* were observed in the lung tissue of AA mice. The knockdown of *INSR* results in the inhibition of inflammation, improvement in airway remodeling, alleviation of airway hyperviscosity, and restoration of Th17/Treg imbalance through the inactiva-

tion of JAK2/STAT3 signaling. These findings collectively suggest that the down-regulation of *INSR* contributes to delaying the progression of AA.

Availability of Data and Materials

The datasets analyzed during the current study are available.

Author Contributions

XLJ contributed to the conception of the study and wrote the manuscript. XLJ and JW performed the experiment. JW contributed to data collection and manuscript preparation. XLJ and JW helped the analysis. Both authors have been involved in revising it critically for important intellectual content. Both authors had reviewed the manuscript and approved the manuscript. Both authors agreed to be accountable for all aspects of the work in ensuring that questions related to the accuracy or integrity of any part of the work are appropriately investigated and resolved.

Ethics Approval and Consent to Participate

The study was conducted to compliance with the Revised Animals guidelines. All experimental protocols of this study were approved by the Ethics Committee of Beijing Biocisco Biomedical Technology Co., Ltd. (Beijing, China) (No. MDL 2022-07-25-01).

Acknowledgment

Not applicable.

Funding

This research received no external funding.

Conflict of Interest

The authors declare no conflict of interest.

References

[1] Incorvaia C, Masieri S, Cavaliere C, Makri E, Sposato B, Frati F. Asthma associated to rhinitis. Journal of Biological Regulators and Homeostatic Agents. 2018; 32: 67–71.

[2] Komlósi ZI, van de Veen W, Kovács N, Szűcs G, Sokolowska M, O'Mahony L, *et al*. Cellular and molecular mechanisms of allergic asthma. Molecular Aspects of Medicine. 2022; 85: 100995.

[3] Enilari O, Sinha S. The Global Impact of Asthma in Adult Populations. Annals of Global Health. 2019; 85: 2.

[4] Reddel HK, FitzGerald JM, Bateman ED, Bacharier LB, Becker A, Brusselle G, *et al*. GINA 2019: a fundamental change in asthma management: Treatment of asthma with short-acting bronchodilators alone is no longer recommended for adults and adolescents. The European Respiratory Journal. 2019; 53: 1901046.

[5] Huang K, Yang T, Xu J, Yang L, Zhao J, Zhang X, *et al*. Prevalence, risk factors, and management of asthma in China: a national cross-sectional study. Lancet (London, England). 2019; 394: 407–418.

[6] Serebrisky D, Wiznia A. Pediatric Asthma: A Global Epidemic. Annals of Global Health. 2019; 85: 6.

[7] Liao X, Wang X, Wang F. The prevalence of asthma among adults in China: a meta-analysis. Chinese Journal of Evidence-Based Medicine. 2020; 20: 1164–1172. (In Chinese)

[8] Sposato B, Scalese M, Milanese M, Masieri S, Cavaliere C, Ricci A, *et al*. Should omalizumab be used in severe asthma/COPD overlap? Journal of Biological Regulators and Homeostatic Agents. 2018; 32: 755–761.

[9] Payankaulam S, Raicu AM, Arnosti DN. Transcriptional Regulation of *INSR*, the Insulin Receptor Gene. Genes. 2019; 10: 984.

[10] Hubbard SR. The insulin receptor: both a prototypical and atypical receptor tyrosine kinase. Cold Spring Harbor Perspectives in Biology. 2013; 5: a008946.

[11] Saltiel AR, Kahn CR. Insulin signalling and the regulation of glucose and lipid metabolism. Nature. 2001; 414: 799–806.

[12] Chen F, Song J, Ye Z, Xu B, Cheng H, Zhang S, *et al*. Integrated Analysis of Cell Cycle-Related and Immunity-Related Biomarker Signatures to Improve the Prognosis Prediction of Lung Adenocarcinoma. Frontiers in Oncology. 2021; 11: 666826.

[13] El-Aarag SA, Mahmoud A, Hashem MH, Abd Elkader H, Hemeida AE, ElHefnawi M. In silico identification of potential key regulatory factors in smoking-induced lung cancer. BMC Medical Genomics. 2017; 10: 40.

[14] Teng Y, Ding Y, Zhang M, Chen X, Wang X, Yu H, *et al*. Genome-wide haplotype association study identifies risk genes for non-small cell lung cancer. Journal of Theoretical Biology. 2018; 456: 84–90.

[15] Zayed H. Novel Comprehensive Bioinformatics Approaches to Determine the Molecular Genetic Susceptibility Profile of Moderate and Severe Asthma. International Journal of Molecular Sciences. 2020; 21: 4022.

[16] Zhu F, Wang KB, Rui L. STAT3 Activation and Oncogenesis in Lymphoma. Cancers. 2019; 12: 19.

[17] Johnson DE, O'Keefe RA, Grandis JR. Targeting the IL-6/JAK/STAT3 signalling axis in cancer. Nature Reviews. Clinical Oncology. 2018; 15: 234–248.

[18] Li H, Bi Q, Cui H, Lv C, Wang M. Suppression of autophagy through JAK2/STAT3 contributes to the therapeutic action of rhynchophylline on asthma. BMC Complementary Medicine and Therapies. 2021; 21: 21.

[19] Ren Y, Liu Y, Wang S, Lei Z, Yan Y, Guan X, *et al*. Zhike pingchuan granules improve bronchial asthma by regulating the IL-6/JAK2/STAT3 pathway. Experimental and Therapeutic Medicine. 2021; 22: 899.

[20] Bai H, Xue Z, Zhang W, Feng C, Zhou Z, Hu S, *et al*. α-Asarone alleviates allergic asthma by stabilizing mast cells through inhibition of ERK/JAK2-STAT3 pathway. BioFactors (Oxford, England). 2023; 49: 140–152.

[21] Liu W, Chen Y, Zeng G, Yang T, Song W. INSR mediated by transcription factor KLF4 and DNA methylation ameliorates osteoarthritis progression via inactivation of JAK2/STAT3 signaling pathway. American Journal of Translational Research. 2020; 12: 7953–7967.

[22] Wang C, Tang J, Qian B, Zeng Z, Gao Y, Song JL. Rubusoside alleviates the ovalbumin-induced mice allergic asthma by modulating the NF-κB activation. Journal of Food Biochemistry. 2020; 44: e13187.

[23] Qian J, Ma X, Xun Y, Pan L. Protective effect of forsythiaside

A on OVA-induced asthma in mice. European Journal of Pharmacology. 2017; 812: 250–255.

[24] Boonpiyathad T, Sözener ZC, Satitsuksanoa P, Akdis CA. Immunologic mechanisms in asthma. Seminars in Immunology. 2019; 46: 101333.

[25] Liu G, Cooley MA, Nair PM, Donovan C, Hsu AC, Jarnicki AG, *et al*. Airway remodelling and inflammation in asthma are dependent on the extracellular matrix protein fibulin-1c. The Journal of Pathology. 2017; 243: 510–523.

[26] Kaur R, Chupp G. Phenotypes and endotypes of adult asthma: Moving toward precision medicine. The Journal of Allergy and Clinical Immunology. 2019; 144: 1–12.

[27] Rabe KF, Calhoun WJ, Smith N, Jimenez P. Can anti-IgE therapy prevent airway remodeling in allergic asthma? Allergy. 2011; 66: 1142–1151.

[28] Finotto S. Resolution of allergic asthma. Seminars in Immunopathology. 2019; 41: 665–674.

[29] Fang L, Sun Q, Roth M. Immunologic and Non-Immunologic Mechanisms Leading to Airway Remodeling in Asthma. International Journal of Molecular Sciences. 2020; 21: 757.

[30] Haeusler RA, McGraw TE, Accili D. Biochemical and cellular properties of insulin receptor signalling. Nature Reviews. Molecular Cell Biology. 2018; 19: 31–44.

[31] Tsai S, Clemente-Casares X, Zhou AC, Lei H, Ahn JJ, Chan YT, *et al*. Insulin Receptor-Mediated Stimulation Boosts T Cell Immunity during Inflammation and Infection. Cell Metabolism. 2018; 28: 922–934.e4.

[32] Cellat M, Kuzu M, İşler CT, Etyemez M, Dikmen N, Uyar A, *et al*. Tyrosol improves ovalbumin (OVA)-induced asthma in rat model through prevention of airway inflammation. Naunyn-Schmiedeberg's Archives of Pharmacology. 2021; 394: 2061–2075.

[33] Campbell L, Hepworth MR, Whittingham-Dowd J, Thompson S, Bancroft AJ, Hayes KS, *et al*. ILC2s mediate systemic innate protection by priming mucus production at distal mucosal sites. The Journal of Experimental Medicine. 2019; 216: 2714–2723.

[34] Hu Y, Chen Z, Zeng J, Zheng S, Sun L, Zhu L, *et al*. Th17/Treg imbalance is associated with reduced indoleamine 2,3 dioxygenase activity in childhood allergic asthma. Allergy, Asthma, and Clinical Immunology: Official Journal of the Canadian Society of Allergy and Clinical Immunology. 2020; 16: 61.

[35] Zou XL, Chen ZG, Zhang TT, Feng DY, Li HT, Yang HL. Th17/Treg homeostasis, but not Th1/Th2 homeostasis, is implicated in exacerbation of human bronchial asthma. Therapeutics and Clinical Risk Management. 2018; 14: 1627–1636.

[36] Lee GR. The Balance of Th17 versus Treg Cells in Autoimmunity. International Journal of Molecular Sciences. 2018; 19: 730.

[37] Kimura A, Kishimoto T. IL-6: regulator of Treg/Th17 balance. European Journal of Immunology. 2010; 40: 1830–1835.

[38] Shi T, Li N, He Y, Feng J, Mei Z, Du Y, *et al*. Th17/Treg cell imbalance plays an important role in respiratory syncytial virus infection compromising asthma tolerance in mice. Microbial Pathogenesis. 2021; 156: 104867.

[39] Jin B, Zhang C, Geng Y, Liu M. Therapeutic Effect of Ginsenoside Rd on Experimental Autoimmune Encephalomyelitis Model Mice: Regulation of Inflammation and Treg/Th17 Cell Balance. Mediators of Inflammation. 2020; 2020: 8827527.